Catalysis Science & Technology

Accepted Manuscript

ROYAL SOCIETY OF CHEMISTRY

rsc.li/catalysis

View Article Online
DOI: 10.1039/C6CY02702D

Catalysis Science & Technology

ARTICLE

W_2C Nanorods with Various Amounts of Vacancy Defects: Determination of Catalytic Active Sites in Hydrodeoxygenation of Benzofuran†

Received 00th January 20xx,
Accepted 00th January 20xx

DOI: 10.1039/x0xx00000x

www.rsc.org/

Rong Liu,[a] Min Pang,[b] Xiaozhen Chen,[b] Chuang Li,[b] Chunjian Xu,*[, a] Changhai Liang*[, b]

Transition metal carbides have been of great interest because of their noble-metal-like properties. Because of the complexity of their structures, it is crucial to design an experiment that can eliminate the influence of supports, surface carbon contamination and particle sizes when finding the exact catalytic active sites. In this work, phase-pure W_2C nanorods (lengths of 2-4μm and diameters of 100-600 nm) with different amounts of crystal defects were prepared by pyrolysis of metatungstate and melamine hybrid nanorods with nanoscale periodic structure synthesized in the aqueous phase. The nanoscale alternating structure between tungsten oxide and melamine effectively promotes the reduction of tungsten oxide and the formation of tungsten carbide, avoiding the deposition of carbon on the surface. At the same time, vacancy defects are generated due to the deficiency of carbon. High pyrolysis temperature (900 °C), prolonged pyrolysis time (4 h), introduction of hydrogen and proper increase of temperature ramping rate (5 °C/min) are favorable to the formation of vacancy defects. The activity of different catalysts was evaluated by the hydrodeoxygenation of benzofuran at 320 to 350 °C. The results show that the vacancy defect sites in W_2C are the key to the high reactivity of W_2C. The vacancy defect sites have favorable properties on the cleavage of carbon-oxygen bonds. $C_{aromatic}$-O bond is cleaved in the case of unsaturated aromatic ring, thereby reducing the consumption of hydrogen. In addition, it is found that the apparent activation energy of each chemical bond is linear-like positively related to its bond dissociation energy.

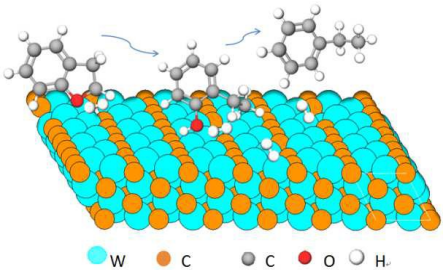

1. Introduction

Since Levy and Boudart[1] found that tungsten carbides display platinum-like behavior in a series of catalytic reactions, early transition metal carbides (TMCs) have been investigated for decades in the fields of catalysis. Extensive studies have shown that early TMCs are catalytically active for reactions such as hydrogenation,[2] hydrogenolysis,[3] dehydrogenation,[4] isomerization,[5] methane to syngas,[6] ammonia decomposition,[7] deoxygenation,[8-11] hydrogen evolution reaction,[12-14] and oxygen reduction reaction.[15, 16] A number of studies[7, 17-19] about relationship of the structure and catalytic behaviors has been performed on experimental or theoretical investigation. Although DFT calculations have drawn attention to the possible role of defects and termination plane upon surface chemistry, experimental studies have seldom addressed this issue and the elucidation of structure–activity relationships for these materials is generally lacking.[20] It is also important to recognize that real catalyst surfaces can be very different from the ideal model surfaces used in calculations. TMCs have proven to be a class of challenging materials to work with due to complications related to (i) phase purity, (ii) surface carbon, (iii) surface termination, (iv) surface oxides, (v) surface defects, and (vi) surface roughness/area.[21] The catalytic activity of TMCs has been influenced by all these factors. Being able to decouple the influences of these six variables is of utmost importance for understanding and optimizing the catalytic performance of TMCs.[21] Until now, no systematic experiment has been carried out to find out the exact highly active catalytic sites with serial pure TMCs which can exclude the impacts of supports, outside carbon layers and particle sizes. Herein it is the key issue to develop a synthetic method that can produce single phase TMCs with high purity and various amounts of defects, then determine the active sites in catalysis.

Generally, based on the direction of carbon diffusion, synthetic methods for TMC can be classified into two

[a] State Key Laboratory of Chemical Engineering, Chemical Engineering Research Center, and School of Chemical Engineering and Technology, Tianjin University, Tianjin 300072, China. E-mail: cjxu@tju.edu.cn; Fax: +86 22 27892145
[b] Laboratory of Advanced Materials and Catalytic Engineering, School of Chemical Engineering, Dalian University of Technology, Dalian 116024, China. E-mail: changhai@dlut.edu.cn; Fax: +86 411 84986353

† Electronic Supplementary Information (ESI) available. See DOI: 10.1039/x0xx00000x

View Article Online
DOI: 10.1039/C6CY02702D

categories, namely, "outside-in" and "inside-out" processes. The former one is typically the temperature-programmed reduction (TPRe) method, in which a mixture of hydrogen and carbon-containing gas, such as CH_4, C_2H_6, or CO, induced the carburization of the corresponding metal oxides or metal. In this way, it is difficult to engineer TMC nanoparticles with controlled properties because the high synthesis temperatures (above 700°C) easily lead to polymeric carbon formation and contamination at the surface of TMC particles, which severely reduces the active sites of the catalyst.[22] In recent years, synthetic routes of carbides have been developed to reduce the surface carbon.[23, 24] One typical example is the carbothermal hydrogen reduction route[25], which leads to less carbon deposition by applying solid carbon during the pyrolysis. However, pure bulk TMC nanoparticles cannot be obtained.

Recently, several new routes were reported that nanostructured TMCs can be generated. W_2C microspheres were synthesized by heating mixtures of ammonium metatungstate salt (AMT) (a tungsten precursor) and resorcinol–formaldehyde polymer (a carbon precursor) for 1 hour in an argon flow and 2 hours in hydrogen flow.[26] Multiple phases of molybdenum carbide were acquired by thermally decomposing a templated precursor, which was precipitated from an aqueous solution of ammonium molybdate and 4-Cl-o-phenylenediamine or p-phenylenediamine by adjusting the pH below 3.[13] Nanostructured transition metal carbides based on the confined carburization in metal-organic frameworks matrix were produced by annealing a compound consisting of copper-based metal-organic frameworks host and molybdenum-based polyoxometalates guest.[12] These methods represent significant advances in TMCs synthesis, which can be considered as "inside-out" process, during which the carbon species diffuse from the bulk to the external surface. Instead of forming coke, most of the carbon species are removed by the hot carrier gases (e.g., Ar, N_2) when reaching the gas-solid interface. Although these nanostructured TMCs show high catalytic performance due to their clean surface and special structures, all of them contain amorphous carbon inside and are also not phase-pure bulk TMCs.

In this work, an organic-inorganic hybrid strategy to obtain tungsten carbide (W_2C) nanorods is designed with varied amounts of defects. In a typical synthesis (Scheme 1), a hybrid was precipitated from an aqueous solution of $(NH_4)_6 H_2W_{12}O_{40}$*nH_2O and melamine at 90°C. The hybrid was pyrolyzed at 750°C for 1h with ramping rate 2 °C/min in an argon flow. The amounts of defects were tuned by changing the treating temperature, time or the gas atmosphere.

Then the W_2C nanorods were studied in the catalytic hydrodeoxygenation of benzofuran, in which the process of hydrogenation, hydrogenolysis, deoxygenation can be studied at the same time. Also we chose hydrodeoxygenation of benzofuran for another important reason that the majority of the biomass-derived molecules contain either a phenolic[27-29] or a furanic structure.[30, 31] Catalytic deoxygenation is playing an important role in the conversion of biomass because most of them have relatively high oxygen content, limiting their direct application as a high grade fuel.[32-34] In a background that research on the conversion of biomass has been motivated by the desire to replace fossil fuels and to mitigate CO_2 emissions and the associated global warming,[35-38] it is meaningful to study the active sites of TMCs for its effective catalysis for hydrogenation and deoxygenation.[9, 10, 39]

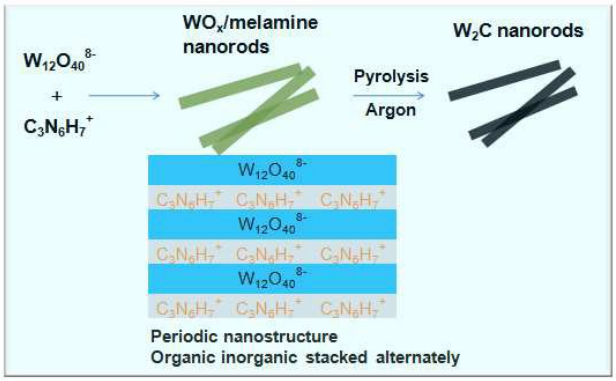

Scheme 1. Illustration for Synthesis of W_2C Nanorods

2. Experimental

2.1. Synthesis of the tungsten-based inorganic-organic hybrid

All solvents and reagents were used as received. A precursor to W_2C was prepared by simply dissolving 0.43 g of melamine and 1 g of $(NH_4)_6 H_2W_{12}O_{40}$*nH_2O with 150 mL of distilled water at 70 °C under magnetic stirring and then the solution was stirred at 90 °C for 12 hours with white suspension formed slowly. Then the product was collected from the suspensions by centrifugation, washed with ethanol and dried in an oven at 80 °C for 24 hours.

2.2. Pyrolysis of the tungsten-based inorganic-organic hybrid

Pyrolysis of the organic- inorganic hybrid (1g) was conducted in a quartz boat placed in a quartz tube reactor. After expelling air by argon at room temperature for 3 hours, the temperature was increased linearly to the target temperature at 2 °C/min or 5 °C/min with flowing argon (70 mL/min) . After the obtained product had been cooled slowly to room temperature, the gas was switched off to allow the slow diffusion of air back into the tube to passivate the carbide surface to avoid bulk oxidation. For the convenience of presentation, the products of the heat treatment of the hybrid conducted in Ar and Ar/H_2 at A °C/min to B °C and held at B °C for C h are denoted as Ar-A-B°C–Ch and Ar/H_2-A-B°C–Ch, respectively. After the annealing and etching processes, the sample was obtained as black powders.

2.3. Hydrodeoxygenation of benzofuran

The hydrodeoxygenation of benzofuran was carried out in a fixed-bed stainless steel reactor (12 × 2 × 500 mm). Toward this end, 0.2 g of catalyst diluted with 2g of quartz sand was loaded into the isothermal section of the reactor and reduced in 4 MPa H_2 (flow rate of 50 mL/min) at 400 °C for 2 h to

View Article Online
DOI: 10.1039/C6CY02702D

remove the surface oxides. A 3 wt % solution of benzofuran in n-decane was introduced after the reactor had cooled to 340°C. The conditions were set as a total pressure of 4 MPa, and a H_2/oil volume ratio of 1000:1. Liquid samples were collected at 1h interval after a stabilization period of 3 h. The effluent composition was analyzed by an Agilent 7890-II gas chromatograph equipped with an OV-101 capillary column (5 m) and a flame ionization detector. It was confirmed that the reaction was not controlled by the internal diffusion by Weisz–Prater Criterion for Internal Diffusion (shown at the bottom of supporting information).

2.4. Characterization

X-ray diffraction (XRD) patterns were taken on a Rigaku D/MAX 2400 diffractometer with Cu Kα(40 kV, 100 mA) radiation. The nitrogen and carbon contents were studied by an Elementar Vario ELsystem. The morphology of the solid powder was obtained on scanning electron microscopy (SEM) using a NOVA NanoSEM 450 system. Transmission electron microscopy (TEM) was performed using Philips CM200 FEG transmission electron microscope (accelerating voltage 200 kV) using high-resolution imaging and energy-dispersive X-ray spectroscopy (EDX). Fourier transform infrared spectra was performed at room temperature on a Nicolet Impact 410 spectrometer with a spectral resolution of 4 cm^{-1}. Raman investigation was performed on a DXR Microscope spectrometer with an excitation wavelength of 514 nm at room temperature. The Brunauer–Emmett–Teller (BET) surface area was studied by static nitrogen physisorption at 77 K subsequent to outgassing at 300 °C until the pressure was lower than 5 mbar. XPS measurements were carried out in an ultrahigh-vacuum setup equipped with a Gammadata-Scienta SES 2002 analyzer. Thermal decomposition of the tungsten-based inorganic-organic hybrid was performed with a Cahn TG-2131 thermo-balance in pure argon or air at a heating rate of 5 °C/min from room temperature to 900℃. The outlet was coupled with a HP 5973 quadrupole mass spectrometer through a silica capillary tube heated to 200℃ to prevent condensation. Multiple signals were monitored at m/ z = 17, 18, 28, and 44, corresponding to NH_3, H_2O, CO/N_2, and CO_2 species respectively.

3. Results and discussion

3.1. Reaction of $(NH_4)_6H_2W_{12}O_{40}$*nH_2O with Melamine

Comparing the XRD patterns (Fig. S1) of $(NH_4)_6H_2W_{12}O_{40}$*nH_2O and the product obtained from reactions between melamine and $(NH_4)_6H_2W_{12}O_{40}$*nH_2O, a new series of peaks occurred at the low 2θ angle for the product and the peaks due to air-dried $(NH_4)_6H_2W_{12}O_{40}$*nH_2O disappeared. The sharp peak, centered at 7.51° in the low 2θ range is characteristic of a highly ordered nanostructure.[40] Corresponding to its d-value, the interlayer distance was determined to be 1.175 nm. The uniform periodic lattice (1.175 nm) was clearly identified by a high-resolution transmission electron microscope (TEM, Fig. S2). Accordingly, the constant interlayer distance has to be a direct consequence of an ordered arrangement of the organic molecules between the inorganic lattices. The nanorod morphology of the hybrid with lengths of 2-5μm and diameters of 200-800nm was well-observed by scanning electron microscope (SEM, Fig. S3). In addition, the hybrid components of melamine and tungstate in the nanorods have also been confirmed by Infrared spectroscopy (FT-IR) (Fig. S4) and CHN elemental analysis in conjugation with thermogravimetry conducted in air (Fig. S5 and Table S3), showing that the hybrid contained 23.0 wt% N, 9.6 wt% C, 1.9 wt% H, and 49.2 wt% W.

3.2. Characterization of W_2C

As the inorganic-organic hybrid is periodic nanostructures in which the inorganic W-O layers and the organic species (melamine iron) are stacked alternately, such a chemical intimacy significantly facilitates the process of oxidation – reduction and formation of carbide in the preparation of W_2C. Heat treatment of the hybrid under argon resulted in well-crystallized pure phase W_2C at 750 °C (See XRD, Fig. 1). The diffraction peaks due to W_2C can be detected at 700 °C (Fig. S6a). Although the products were dominated by W_2C at 800 °C or higher temperatures, a trace amount of metal tungsten was detected by XRD and its amount was increased with temperature (Fig. S6b and table S3). By further increasing to 900 °C, the new diffraction peaks at 35.44 and 48.16° were observed which can be attributed to WC (Fig. S6b). When the heat rate changed to 5 °C /min, the diffraction peaks due to W_2C also can be detected at 700 °C (Fig. 6Sc), but a trace of metal tungsten started to appear even at 750 °C and more metal tungsten (Fig. 6Sd) was produced comparing to that of using 2°C/min at the corresponding temperature (Table S3), which is attributed to the character of "inside-out" processes that the carbon diffusion speed is not fast enough to supply carbons for the forming of W_2C on the surface when temperature ramping speed is high. In such a condition, the more tungsten in the surface means the more vacancy defects due to a lack of carbon atom (See dark spots in red circles, HRTEM, Fig. 2 and S25).

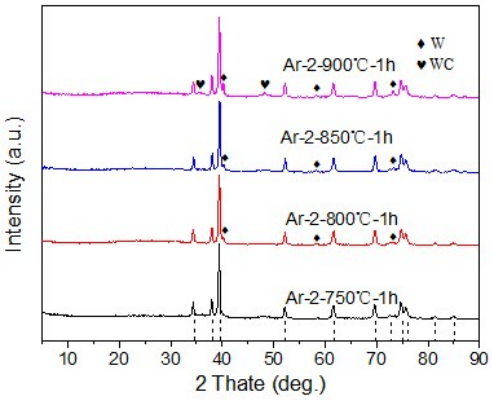

Fig. 1. XRD patterns of W_2C originating from the heat treatment of the hybrid at different conditions. The standard pattern of W_2C (PDF# 35-0776) is shown (dashed lines) at the bottom.

View Article Online
DOI: 10.1039/C6CY02702D

The pyrolysis products obtained, similar to the hybrid, appear to be thinner nanorods with lengths of 2-4μm and diameters of 100-600 nm (See SEM, Fig. 2a, S7, S8 and S9). No residual carbon was detected in W_2C nanorods by Raman spectra (Fig. S10) and HRTEM of W_2C (Fig. S25). Only W, C and O signals were detected by the energy dispersive spectroscopy attached on SEM (Fig. S11), with the small signal of O being due to the surface oxidation of W_2C. The uniform distribution of W and C elements is illustrated by EDX elemental mapping images (Fig. S11). The atomic ratios of W to C in all of the W_2C products determined by CHN elemental analysis and TG were about 2 (Table S2), equal to the theoretical value in W_2C.

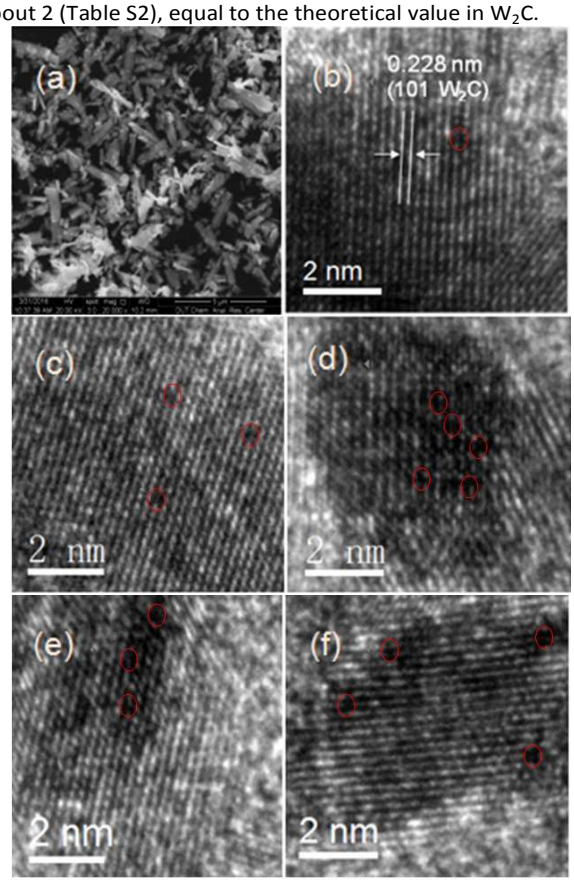

Fig. 2. SEM image of (a) Ar-2-750°C-1h and high-resolution TEM images of samples: (b) Ar-2-750°C-1h; (c) and (d) Ar-2-900°C-1h; (e) and (f) Ar-2-750°C-1hH_2

The W-4f XPS spectra of Ar-2-750°C-1h (Fig. 3), Ar-2-750°C-4h and Ar-2-900°C-1h (Fig. S12) confirmed that W were present in the W_2C and WO_3 state at the surface. The tungsten carbide/oxide surface ratios in the three samples were all estimated to be about 64:36. It is believed that some part of surface W_2C was oxidized in air after preparation. It was also certified that there was very little amount of residual N at the surface of W_2C nanorods because of the absence of sharp peaks in N 1s (Fig. S13).

The BET surface areas of the products distributed from 18.5m^2/g (Ar-2-750°C-1h) to 14.7m^2/g (Ar-2-900°C-1h) (Fig. S14 and Table S2) and the differences from each other were small. Also TEM images (Fig. S25) showed that they had similar surface structures, so that they had very little differences in surface roughness. The smaller surface area of Ar-2-900°C-1h is attributed to the aggregation of some W_2C nanorods at higher temperature (Fig. S9). The pore-size distribution (average pore diameter =8.1nm) of Ar-2-750°C-1h (Fig. S14) indicates that there are abundance of mesopores and very few micropores in the W_2C nanorods. The small surface area and the shortage of micropores are further evidences of high purity of W_2C nanorods. For unsupported carbide, a high surface area typically comes from amorphous carbon, unless there are special well-developed pore structures. Since the products are phase-pure W_2C with high purity, the BET surface area could be considered as the intrinsic area value of a perfect W_2C surface for catalytic reaction.

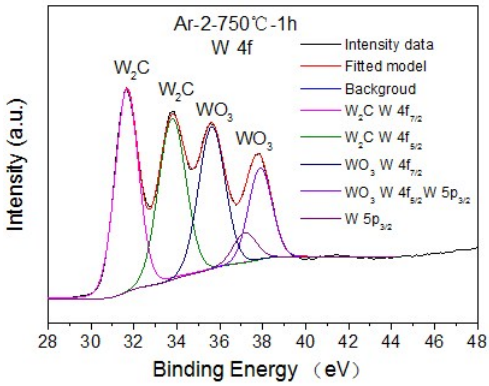

Fig. 3. XPS W 4f spectra of Ar-2-750°C-1h

3.3. Formation mechanism of W_2C

In order to understand how the conversion from the hybrid to W_2C was carried out in detail, the gases evolved during the heat treatment in argon were monitored using an on-line mass spectrometer to provide insight into the reaction pathway.

TG curve and MS curves (Fig. S23) are divided into four regions. The first region in the range of 100 – 270 °C represents the vaporization of physically adsorbed water and the slow dehydration of the hybrid. The second step starting from about 320 °C is mainly attributed to the triggered sublimation and decomposition of melamine. The sublimated melamine can be observed in the inner wall of the quartz tube after heat treatment. The initial decomposition of melamine and the reduction of WO_x begin to occur. Some of the O and N atoms are removed through its combination with the neighboring H to form H_2O and NH_3 with a peak maximum at 390 °C. In the third region, the further decomposition of melamine and the degradation of WO_x by C are in progress with forming NH_3, CO / N_2 and CO_2 after 400 °C. With a peak at 425 °C, the NH_3 released at higher temperature is considered to be due to the pyridine N of melamine. The elimination of O and N is intensified through the formation of CO/N_2 (peak at 500°C) and an appreciable amount of CO_2 (peak at 440°C). After 600°C, it is considered as the last region in which the residue C, N and W are combined together. The relatively stable WC_xN_y is formed and then transform to W_2C when temperature is higher than 700°C (XRD, Fig. S6). Based on the CHN analysis data, after 650°C, the overall atom ratio W : C

View Article Online
DOI: 10.1039/C6CY02702D

keeps to be at 2 and N : W decreases with increasing temperature. Then it can be concluded that N is removed in the form of N_2 as temperature climbs up. Consequently, vacancy sites are formed with the removal of N because there is not enough carbon to replenish. Furthermore, almost no carbon species are formed after 600°C, which is the reason for the undetected residue carbon at the surface of W_2C. The whole process of the conversion from the hybrid to W_2C is summarized in these transformations:

$$(C_3H_7N_6)_8W_{12}O_{40}{*}4H_2O \xrightarrow[\text{Argon}]{25\text{ to }700℃} WC_xN_y+C_3H_6N_6+H_2O+NH_3+CO_2+CO+N_2$$
$$WC_xN_y \xrightarrow[\text{Argon}]{>700℃} W_2C+N_2$$

Because the direction of carbon diffusion is inside to out, N is removed in the form of N_2 at high temperature and melamine ($C_3H_6N_6$) is component rich of N and short of C, a variety of W_2C catalysts with different amounts of vacancy defects are obtained by controlling pyrolysis process. Meanwhile, as it is thermodynamically favored to form metal terminated surfaces under low carburizing potentials,[8] the favorable surface termination of the obtained W_2C should be W-terminated surface under argon environment and the "inside to out" processes of carbon diffusion.

We also tried to improve the removal of carbonitride by replacing the inert gas argon with the mixture of argon and a small amount of hydrogen. Not as expected, metal tungsten was obtained at 650 °C, 750 °C and 800 °C (Fig. S15), which may be the result of carbon-hydrogenating at elevated temperatures. Then another new way to create more vacancy defects was found, that is, to keep the pyrolysis process the same as Ar-2-750°C-1h before it get to 750°C and only switch the inert gas to the mixture of argon (70 mL/min) and hydrogen (35 mL/min) when it get to 750°C and keep for 1h. Denote the product as Ar-2-750°C-1hH_2. Its phase is W_2C with a small amount of metal W (XRD, Fig. S16), which also improve that the carbon atoms in the compound are already very stable and have strong binds with tungsten atoms when the temperature comes to 750°C.

3.4. Hydrodeoxygenation of benzofuran over W_2C catalysts

By analyzing the product distributions as a function of contact time at different temperatures on a variety of W_2C catalysts (Fig. S17), the reaction pathway was proposed (Scheme 2, bold lines represent the major pathway). After the furan double bond was saturated (denote this step as Conv), the C–O –C bond was selectively cleaved at the position of the aliphatic carbon (denoted as COC). Then it is followed by the cleavage of the aromatic carbon and oxygen atom (denoted as DO), and the resulting deoxygenated product is progressively hydrogenated. At the same time the whole process is accompanied by a small amount of C-C bond cleavages (denoted as CCC).

The reaction pathway is completely different from the one over the noble metal catalysts in which the benzene rings are firstly saturated followed by deoxygenation (Scheme S1).[41] Because of the difference, W_2C has resulted in higher aromatics yield and lower hydrogen consumption than that by noble metals.

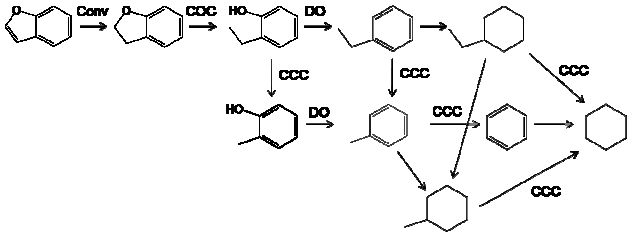

Scheme 2. The reaction pathway of benzofuran hydrodeoxygenation over W_2C catalysts

In view of the proposed reaction pathway, the following rates (reacted molecules per cm^2 catalyst surface per second) is defined: R_{Conv} represents the number of double bonds being hydrogenated, i.e. the conversion number of benzofuran; R_{COC} represents the cleavage number of C-O-C; R_{DO} represents the cleavage number of the aromatic carbon and oxygen bonds (marked as C_{ar}-O), i.e. the amount of deoxygenation. R_{CCC} represents the cleavage number of C-C; R_{H2} represents the number of hydrogen reacted (because hydrogen participated in each process, calculating the rate of consumed hydrogen can later be used to describe the average reaction rate of the whole process, which also indicates the activity of the catalyst).

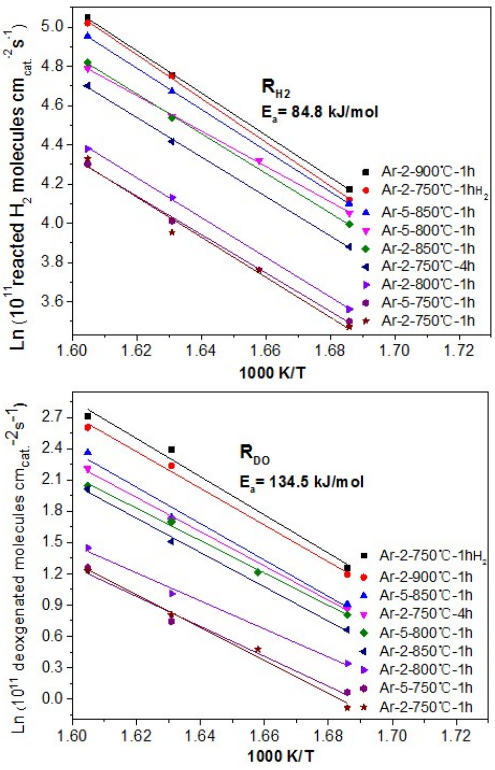

Fig. 4. Arrhenius plots for R_{H2} and R_{DO} on different W_2C catalysts.

Fig. S18 shows that with increasing contact time, the overall hydrogen reaction rate (R_{H2}) was almost constant while the

View Article Online
DOI: 10.1039/C6CY02702D

deoxygenation rate （R_{DO}） was increased apparently, indicating that there is competition between hydrodeoxygenation reaction and other hydrogenation reactions, and they have some common catalytic active sites.

Those catalysts showed almost equal apparent activation energy at each major reaction step (see Arrhenius plots in Fig. 4 and Fig. S19), showing that they all had the same active sites.

Comparing the R_{H2} of different catalysts(Fig. 5), the overall catalytic activity order is as follows: Ar-2-900°C-1h > Ar-2-750°C-1hH_2 > Ar-5-850°C-1h > Ar-5-800°C-1h, Ar-2-850°C-1h > Ar-2-750°C-4h > Ar-2-800°C-1h > Ar-5-750°C-1h, Ar-2-750°C-1h. Comparing the R_{DO} (Fig. 5), the deoxygenation activity order is as follow: Ar-2-750°C-1hH_2 > Ar-2-900°C-1h > Ar-5-850°C-1h > Ar-2-750°C-4h, Ar-5-800°C-1h, Ar-2-850°C-1h > Ar-2-800°C-1h > Ar-5-750°C-1h, Ar-2-750°C-1h. The difference in the orders of R_{H2} and R_{DO} may be due to different distributions of active sites.

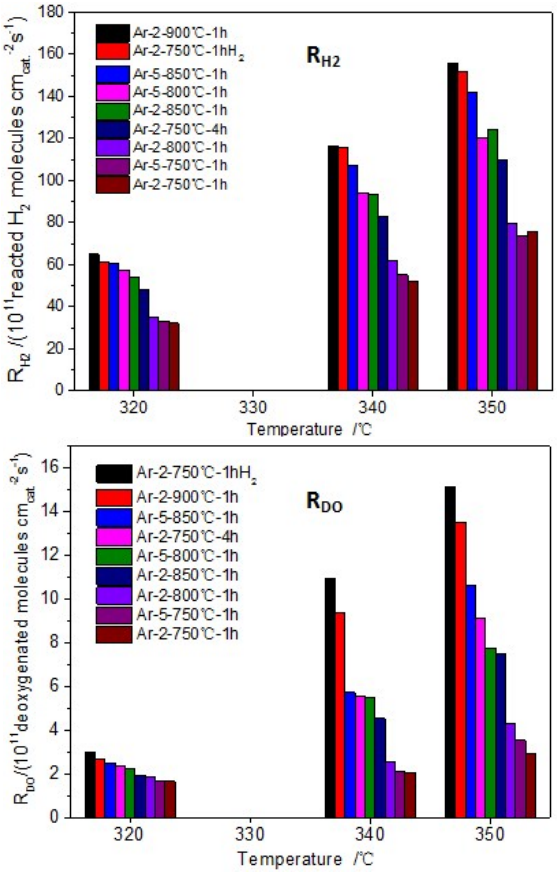

Fig. 5. R_{H2} and R_{DO} at different temperatures on different W_2C catalysts.

The catalytic activity (R_{H2}) of Ar-2-750°C-1h was taken as the reference 1. The relative catalytic activities of each catalyst are shown in Table S3. Ar-2-900°C-1h and Ar-2-750°C-1hH_2 are more than twice as active as Ar-2-750°C-1h. Each catalyst is a pure phase W_2C and has a surface with the same amount of W_2C per unit area. But they show significant differences in activity, so not every W_2C has hydrogenation activities, but there are special active sites which make them active. The difference in catalytic activity was mainly attributed to the difference in the number of these active sites. These specific active sites should have special structures. Based on the HRTEM results of Ar-2-750°C-1h, Ar-2-750°C-4h, Ar-2-900°C-1h and Ar-2-750°C -1hH_2 (Fig. 2 and S25), it was found that the selected W_2C catalysts all contained crystal defects, such as twin boundaries, stacking faults, dislocations, and vacancies. However, the numbers of defects were different, Ar-2-750°C -1h showed a few vacancies, and there were some twin boundaries, stacking faults, dislocations; Besides the line and planar defects, Ar-2-750-4h also showed a little more vacancies, and a large amount of vacancies appeared in Ar-2-900°C-1h and Ar-2-750°C-1hH_2. By counting and calculating the numbers of vacancies on multiple HRTEM images, the statistical average numbers of carbon vacancies per square nanometers of the catalysts were obtained: Ar-2-750°C-1hH_2 (2.5 vacancies/nm^2), Ar-2-900°C-1h (2.6 vacancies/nm^2), Ar-5-800°C-1h (1.7 vacancies/nm^2), Ar-2-750°C-4h (1.6 vacancies/nm^2), Ar-2-750°C-1h (1.1 vacancies/nm^2). It was found that the numbers of vacancies and the levels of catalytic activity were positively correlated (Fig. S26).

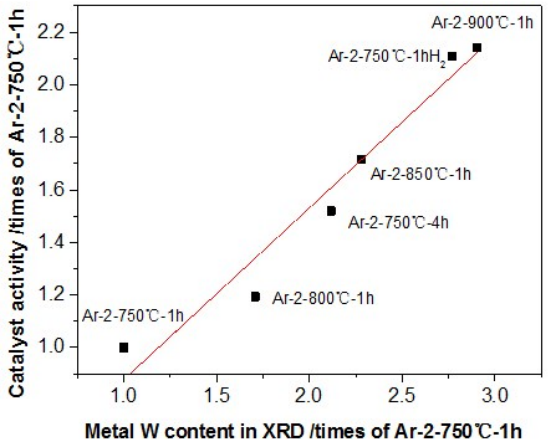

Fig. 6. Relationship between catalytic activity and tungsten content in XRD.

Although XRD results showed diffraction peaks of metal tungsten, the lattice of metallic tungsten had not been found in HRTEM images. In conjunction with the formation mechanism of the W_2C, it is believed that these diffraction peaks come into being by superimposing the diffraction peaks of small tungsten centers dispersed in various localized regions as a result of carbon vacancies. Some of these tungsten atoms can still be considered as defective part of W_2C, and they can also provide more W-termination for the surface of W_2C. It is believed that the increase of vacancy sites and the increase of W-terminated surface is accompanied by each other. The surface termination of carbide also has some impact on the catalysis for hydrodeoxygenation.[8]

The numbers of W_2C defects should be positively correlated with the tungsten contents in XRD which is also positively correlated with the catalytic activity (see Fig. 6). These samples (Ar-5-750°C-1h, Ar-5-800°C-1h and Ar-5-850°C-1h), comparing with each others, also are also correlated, but in comparison

View Article Online
DOI: 10.1039/C6CY02702D

with the samples from temperature ramping speed 2°C/min, they exhibit much higher metal tungsten contents in XRD (Fig. S6 and Table S3). It is believed that the rapid heating rate led to a large number of carbon loss from some locals, resulting in the formation of some large metal tungsten centers. Only a fraction of the tungsten in these large tungsten centers has high activity due to carbon vacancies. When raising the heating rate to 20°C/min, tungsten carbide with a layer of sintered metal tungsten on the outside is an extreme example of the effect of heating rate. The pure metal tungsten (Ar/H_2-2-750°C-1h) obtained by pyrolyzing the hybrid in a mixture of argon and hydrogen was also evaluated by hydrodeoxygenation of benzofuran and it was found that the sample showed very low activity. It is concluded that pure tungsten, which is not associated with W_2C, is not a highly active site.

The R_{H2} and R_{DO} of Ar-2-750°C -1hH_2, which were placed in air at 28°C for 45 days, were reduced to 41% and 9% of the ones of the fresh catalyst respectively (Table S4). And for Ar-2-900°C-1h placed in air at 28°C for 90 days, they were 18% and 6% respectively (Table S4). Although their XRD did not show any difference from the fresh W_2C catalyst, their activity was significantly reduced over time. This may be because the defects are so active that even in the air at room temperature they are gradually oxidized to form tungsten oxide and lose activity. It is also shown that WO_3 formed by surface oxidation is also not a highly active site for the hydrodeoxygenation of benzofuran.

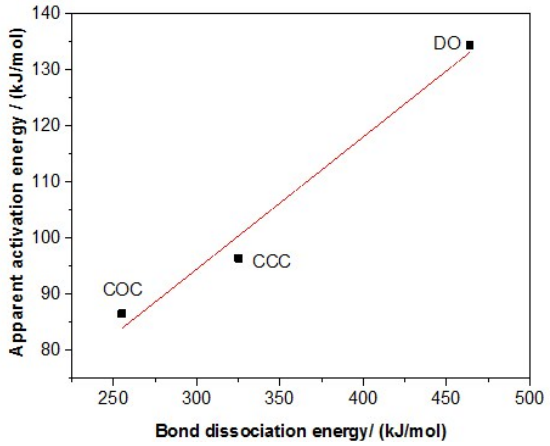

Fig. 7. Relationship between apparent activation energy and bond dissociation energy for COC, CCC and DO.

From the Arrhenius plots (Fig. 4, S19 and S20), the apparent activation energy of each step is obtained in the order: DO (134.5kJ/mol) > CCC (96.4kJ/mol)> COC (86.6kJ/mol)> R_{H2} (84.8kJ/mol)> Conv (68.5kJ/mol). The apparent activation energy of R_{H2} is considered as the average apparent activation energy of the whole process. In combination with the bond dissociation energies of C_{ar}-O, C-C, and C-O (Table S5), it is found that the apparent activation energies of these steps are approximately linearly related to the bond dissociation energies of the chemical bonds (Fig. 7). Therefore, in the future study, the bond dissociation energy can be used as an important reference for the activity of chemical bond cleavage, and it is important for us to judge the effects of temperature on reaction rate and selectivity. The bond dissociation energy of C_{ar}-O is high, so the increase of temperature has a strong influence on the DO process.

The bond dissociation energy of C_{ar}-O (464 kJ·mol^{-1}) is larger than that of cyclo-C_6H_{11}–OH (399kJ·mol^{-1}) after the saturation of the aromatic ring, and therefore the direct deoxygenation requires a higher temperature than the deoxygenation after the saturation of aromatic ring. In addition, although the dissociation energy of C_{ar}-O is larger than that of C-C, the number of C_{ar}-O cleavage is significantly higher than that of C-C cleavage (Fig. S22) under the catalysis of W_2C, indicating that W_2C contains active sites with good scission effect on C_{ar}-O and shows excellent oxophilicity that makes it suitable for deoxygenation (Fig. S21).

3.5. Mechanism of benzofuran hydrodeoxygenation over W_2C catalysts

On the basis of the above results and discussion, the defects on the surface of W_2C, especially the vacancy sites, exhibit high catalytic activity during the hydrodeoxygenation of benzofuran. The furan double bonds are saturated by the dissociated H· atoms on the surface of the W_2C. And then the $C_{aliphatic}$–O–$C_{aromatic}$ linkages are adsorbed on the defects of W_2C, and the cleavage preference is on the weaker $C_{aliphatic}$–O bonds rather than on the stronger C_{ar}–O bonds. The dissociated H· atoms on the W_2C surface are in turn added to form ethyl phenol. After that, the C_{ar}-O bonds in ethyl phenol, prior to the aromatic ring and C-C bond, are adsorbed on tungsten atoms of W_2C with carbon vacancies, and are consequently cleaved and saturated under the synergistic effect of dissociated H· atoms, resulting in the formation of ethylbenzene and water after desorption. C-C is adsorbed on the defects of W_2C in small amount, and then is cleaved and saturated under the action of dissociated H· atoms. At the same time, a small amount of aromatic rings after deoxygenation are saturated while non-deoxygenated molecules need to give priority to the adsorption of oxygen atoms.

4. Conclusions

Metatungstate and melamine hybrid nanorods (lengths of 2-5 μm and diameters of 200-800 nm) with nanoscale periodic structure were synthesized in aqueous phase at 90 °C. During pyrolyzing the hybrid, the nanoscale alternating contact between tungsten oxide and melamine effectively promotes the reduction of tungsten oxide and the carbonization of tungsten and inverts the diffusion direction of carbon to be from inside to outside, thereby avoiding the deposition of carbon on the surface. Meanwhile, carbon and nitrogen are gradually lost. Carbon and tungsten are stoichiometrically combined to form W_2C. Since melamine has less carbon and more nitrogen contents, when nitrogen and carbon are locally lost significantly and there is not enough carbon to complement or timely replenished, vacancy defects will be

View Article Online
DOI: 10.1039/C6CY02702D

generated due to the lack of carbon. Therefore, W_2C nanorods (lengths of 2-4 μm and diameters of 100-600 nm) with different number of vacancy defect sites were obtained by controlling the pyrolysis temperature, pyrolysis time, temperature ramping rate or the introduction of hydrogen. The trace amount of metal tungsten detected by XRD can be still considered as defective part of W_2C due to carbon atom vacancies. High pyrolysis temperature, lengthening pyrolysis time and introduction of proper amount of hydrogen, properly increasing temperature ramping rate are favorable to form more vacancy sites which lead to higher activity in hydrodeoxygenation of benzofuran. Rich vacancy sites in the tungsten carbides exhibit excellent oxophilicity and good scission effect on C_{ar}-O. C_{ar}-O bond is cleaved in the case of unsaturated aromatic ring, thereby reducing the consumption of hydrogen. It is found that the apparent activation energy of each chemical bond cleavage is linearly related to its bond dissociation energy. Therefore, bond dissociation energy can be used as an important reference for chemical bond cleavage process in future studies.

Acknowledgements

We gratefully acknowledge the financial support provided by the National Natural Science Foundation of China (No. 21573031 and 21373038), the Fundamental Research Funds for the Central Universities (DUT15ZD106) and Program for Excellent Talents in Dalian City (2016RD09).

Notes and references

1 R. B. Levy and M. Boudart, *Science*, 1973, **181**, 547-549.
2 M. Pang, C. Liu, W. Xia, M. Muhler and C. Liang, *Green Chem.*, 2012, **14**, 1272.
3 M. K. Neylon, S. Choi, H. Kwon, K. E. Curry and L. T. Thompson, *Appl. Catal. A Gen.*, 1999, **183**, 253-263.
4 L. Leclercq, M. Provost, H. Pastor and G. Leclercq, *J. Catal.*, 1989, **117**, 384-395.
5 F. H. Ribeiro, R. A. D. Betta, M. Boudart, J. Baumgartner and E. Iglesia, *J. Catal.*, 1991, **130**, 86-105.
6 J. B. Claridge, A. P. E. York, A. J. Brungs, C. Marquez-Alvarez, J. Sloan, S. C. Tsang and M. L. H. Green, *J. Catal.*, 1998, **180**, 85-100.
7 W. Q. Zheng, T. P. Cotter, P. Kaghazchi, T. Jacob, B. Frank, K. Schlichte, W. Zhang, D. S. Su, F. Schuth and R. Schlogl, *J. Am. Chem. Soc.*, 2013, **135**, 3458-3464.
8 M. S. Mark, C. Cha-Jung and B. Aditya, Catal. Sci. Technol. 2016. **6**, 602-616.
9 R. W. Gosselink, D. R. Stellwagen and J. H. Bitter, *Angew. Chem. Int. Ed.*, 2013, **52**, 5089-5092.
10 Baddour. G. Frederick, Nash. P. Connor, Schaidle. A. Joshua, Ruddy and A. Daniel, *Angew. Chem. Int. Ed.*, 2016, **55**, 9026-9029.
11 D. R. Stellwagen and J. H. Bitter, *Green Chem.*, 2015, **17**, 582-593.
12 H. B. Wu, B. Y. Xia, L. Yu, X. Y. Yu and X. W. Lou, *Nature Commun.*, 2015, **6**.
13 C. Wan, Y. N. Regmi and B. M. Leonard, *Angew. Chem. Int. Ed.*, 2014, **53**, 6407-6410.
14 D. V. Esposito, S. T. Hunt, A. L. Stottlemyer, K. D. Dobson, B. E. McCandless, R. W. Birkmire and J. G. G. Chen, *Angew. Chem. Int. Ed.*, 2010, **49**, 9859-9862.
15 C. H. Liang, L. Ding, C. A. Li, M. Pang, D. S. Su, W. Z. Li and Y. M. Wang, *Energ. & Environ. Sci.*, 2010, **3**, 1121-1127.
16 X. M. Ma, H. Meng, M. Cai and P. K. Shen, *J. Am. Chem. Soc.*, 2012, **134**, 1954-1957.
17 L. H. Bennett, J. R. Cuthill, A. J. McAlister, N. E. Erickson and R. E. Watson, *Science*, 1974, **184**, 563-565.
18 D. R. Stellwagen and J. H. Bitter, *Green Chem.*, 2015, **17**, 582-593.
19 P. Liu and J. A. Rodriguez, *J. Chem. Phys.*, 2004, **120**, 5414-5423.
20 A. M. Alexander and J. S. J. Hargreaves, *Chem. Soc. Rev.*, 2010, **39**, 4388-4401.
21 D. V. Esposito and J. G. G. Chen, *Energ. & Environ. Sci.*, 2011, **4**, 3900-3912.
22 S. T. Hunt, M. Milina, A. C. Alba-Rubio, C. H. Hendon, J. A. Dumesic and Y. Roman-Leshkov, *Science*, 2016, **352**, 974-978.
23 S. R. Vallance, S. Kingman and D. H. Gregory, *Adv. Mater.*, 2007, **19**, 138-+.
24 A. Celzard, J. F. Mareche, G. Furdin, V. Fierro, C. Sayag and J. Pielaszek, *Green Chem.*, 2005, **7**, 784-792.
25 C. H. Liang, P. L. Ying and C. Li, *Chem. Mater.*, 2002, **14**, 3148-3151.
26 R. Ganesan and J. S. Lee, *Angew. Chem. Int. Ed.*, 2005, **44**, 6557-6560.
27 C. Zhao, Y. Kou, A. A. Lemonidou, X. B. Li and J. A. Lercher, *Angew. Chem. Int. Ed.*, 2009, **48**, 3987-3990.
28 A. Berenguer, T. M. Sankaranarayanan, G. Gomez, I. Moreno, J. M. Coronado, P. Pizarro and D. P. Serrano, *Green Chem.*, 2016, **18**, 1938-1951.
29 D. A. Ruddy, J. A. Schaidle, J. R. Ferrell, J. Wang, L. Moens and J. E. Hensley, *Green Chem.*, 2014, **16**, 454-490.
30 G. Y. Li, N. Li, J. F. Yang, L. Li, A. Q. Wang, X. D. Wang, Y. Cong and T. Zhang, *Green Chem.*, 2014, **16**, 594-599.
31 A. D. Sutton, F. D. Waldie, R. L. Wu, M. Schlaf, L. A. Silks and J. C. Gordon, *Nature Chem.*, 2013, **5**, 428-432.
32 C. Zhao, T. Bruck and J. A. Lercher, *Green Chem.*, 2013, **15**, 1720-1739.
33 H. L. Wang, H. Ruan, H. S. Pei, H. M. Wang, X. W. Chen, M. P. Tucker, J. R. Cort and B. Yang, *Green Chem.*, 2015, **17**, 5131-5135.
34 M. Saidi, F. Samimi, D. Karimipourfard, T. Nimmanwudipong, B. C. Gates and M. R. Rahimpour, *Energ. & Environ. Sci.*, 2014, **7**, 103-129.
35 R. Ma, W. Hao, X. Ma, Y. Tian and Y. Li, *Angew. Chem. Int. Ed.*, 2014, **53**, 7310-7315.
36 N. Ji, T. Zhang, M. Y. Zheng, A. Q. Wang, H. Wang, X. D. Wang and J. G. G. Chen, *Angew. Chem. Int. Ed.*, 2008, **47**, 8510-8513.
37 R. Ooms, M. Dusselier, J. A. Geboers, B. Op de Beeck, R. Verhaeven, E. Gobechiya, J. A. Martens, A. Redl and B. F. Sels, *Green Chem.*, 2014, **16**, 695-707.
38 C. J. Zhu, T. Shen, D. Liu, J. L. Wu, Y. Chen, L. F. Wang, K. Guo, H. J. Ying and P. K. Ouyang, *Green Chem.*, 2016, **18**, 2165-2174.
39 S. A. W. Hollak, R. W. Gosselink, D. S. van Es and J. H. Bitter, *Acs Catal.*, 2013, **3**, 2837-2844.
40 J. Polleux, A. Gurlo, N. Barsan, U. Weimar, M. Antonietti and M. Niederberger, *Angew. Chem. Int. Ed.*, 2006, **45**, 261-265.
41 C. Y. Liu, Z. F. Shao, Z. H. Xiao, C. T. Williams and C. H. Liang, *Energ. & Fuels*, 2012, **26**, 4205-4211.

View Article Online
DOI: 10.1039/C6CY02702D

W_2C Nanorods with Various Amounts of Vacancy Defects: Determination of Catalytic Active Sites in Hydrodeoxygenation of Benzofuran

Rong Liu, Min Pang, Xiaozhen Chen, Chuang Li, Chunjian Xu, Changhai Liang

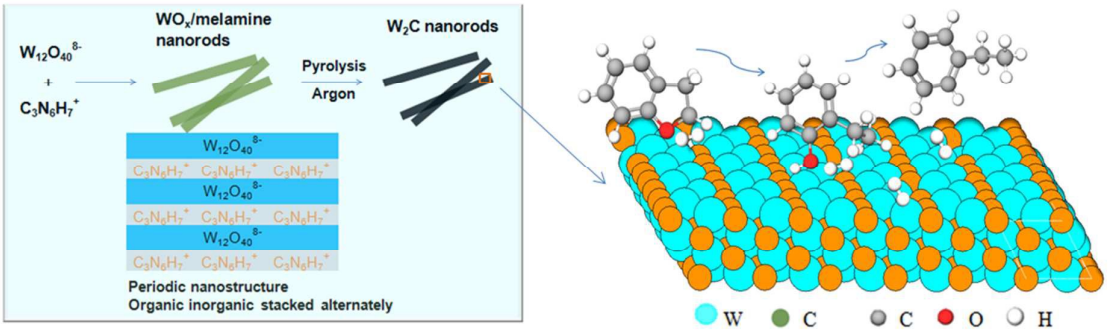

Phase-pure W_2C nanorods were prepared by pyrolysis of metatungstate and melamine hybrid and showed excellent performnce for hydrodeoxygenation of benzofuran.